Anal. Chem. **2003,** *75,* 3806−3816

Quantifying Trace Elements in Individual Aquatic Protist Cells with a Synchrotron X-ray Fluorescence Microprobe

Benjamin S. Twining,*,† Stephen B. Baines,† Nicholas S. Fisher,†,‡ Jörg Maser,§ Stefan Vogt,§ Chris Jacobsen,‡,|| Antonio Tovar-Sanchez,† and Sergio A. Sañudo-Wilhelmy†

Marine Sciences Research Center, Center of Environmental Molecular Science, and Department of Physics and Astronomy, Stony Brook University, Stony Brook, New York 11794, and Experimental Facilities Division, Advanced Photon Source, Argonne National Laboratory, Argonne, Illinois 60439

The study of trace metal cycling by aquatic protists is limited by current analytical techniques. Standard "bulk" element analysis techniques that rely on physical separations to concentrate cells for analysis cannot separate cells from co-occurring detrital material or other cells of differing taxonomy or trophic function. Here we demonstrate the ability of a synchrotron-based X-ray fluorescence (SXRF) microprobe to quantify the elements Si, Mn, Fe, Ni, and Zn in individual aquatic protist cells. This technique distinguishes between different types of cells in an assemblage and between cells and other particulate matter. Under typical operating conditions, the minimum detection limits are 7.0×10^{-16} mol μm^{-2} for Si and between 5.0×10^{-20} and 3.9×10^{-19} mol μm^{-2} for Mn, Fe, Ni, and Zn; this sensitivity is sufficient to detect these elements in cells from even the most pristine waters as demonstrated in phytoplankton cells collected from remote areas of the Southern Ocean. Replicate analyses of single cells produced variations of <5% for Si, Mn, Fe, and Zn and <10% for Ni. Comparative analyses of cultured phytoplankton cells generally show no significant differences in cellular metal concentrations measured with SXRF and standard bulk techniques (spectrophotometry and graphite furnace atomic absorption spectrometry). SXRF also produces two-dimensional maps of element distributions in cells, thereby providing information not available with other analytical approaches. This technique enables the accurate and precise measurement of trace metals in individual aquatic protists collected from natural environments.

Aquatic protists continually accumulate and remineralize elements from the ambient environment, resulting in cellular element stoichiometries that can provide information about the physiological state of the organism, the ambient chemical environment, and the biogeochemical role of the organism within that environment.[1,2] Stoichiometries can also reveal substitution or competition effects between co-occurring cellular trace metals, as have been observed for Fe, Mn, Cd, Co, and Zn in cultures of marine phytoplankton.[3,4] While cell composition and elemental stoichiometry are commonly studied in cultured organisms, it has heretofore been nearly impossible to obtain meaningful metal measurements of individual components of plankton assemblages in natural waters. Standard "bulk" techniques such as graphite furnace atomic absorption spectrometry (GFAAS) or inductively coupled plasma mass spectrometry (ICPMS) generally concentrate cells prior to analysis using physical separations (e.g., filtration or net-tows), which also collect substantial amounts of detrital and mineral particles. Analysis of individual cells isolated from other particles would be preferable. However, GFAAS and ICPMS do not have adequate absolute sensitivity to conduct such single-cell analyses of the bioactive transition metals Mn, Fe, Ni, Cu, and Zn, which often function as cofactors for enzymes.[5] In the case of some oceanic phytoplankters, cellular Fe may not exceed 3×10^{-18} mol,[6] while the absolute Fe detection limit for GFAAS is ~1000-fold higher (7×10^{-15} mol, assuming a sample size of 20 μL).[7] Filtration techniques also preclude the separation of like-sized cells and abiotic particles or cells of varying taxonomy and trophic function, introducing ambiguity into the interpretation of the results. Because of the limitations of bulk size-fractionation techniques, most inferences about oceanic trace metal cycling by protists are from laboratory studies on metal bioaccumulation in monospecific cultures[4,8,9] or from metal concentration profiles in oceanic water columns.[10,11] There are only a few reliable field

* Corresponding author. E-mail: btwining@ic.sunysb.edu.
† Marine Sciences Research Center, Stony Brook University.
‡ Center of Environmental Molecular Science, Stony Brook University.
§ Argonne National Laboratory.
|| Department of Physics and Astronomy, Stony Brook University.

(1) Morel, F. M. M.; Hudson, R. J. M. In *Chemical Processes in Lakes*; Stumm, W., Ed.; John Wiley & Sons: New York, 1985; pp 251−281.
(2) Sterner, R. W.; Elser, J. J. *Ecological Stoichiometry*; Princeton University Press: Princeton, NJ, 2002.
(3) Price, N. M.; Morel, F. M. M. *Nature* **1990**, *344*, 658−660.
(4) Sunda, W. G.; Huntsman, S. A. *Limnol. Oceanogr.* **2000**, *45*, 1501−1516.
(5) Sunda, W. G. *Biol. Oceanogr.* **1988/1989**, *6*, 411−442.
(6) Sunda, W. G.; Huntsman, S. A. *Mar. Chem.* **1995**, *50*, 189−206.
(7) Vandecasteele, C.; Block, C. B. *Modern Methods for Trace Element Determination*; John Wiley & Sons: New York, 1993.
(8) Fisher, N. S. *Limnol. Oceanogr.* **1986**, *31*, 443−449.
(9) Brand, L. E. *Limnol. Oceanogr.* **1991**, *36*, 1756−1771.
(10) Bruland, K. W. In *Chemical Oceanography*; Riley, J. P., Chester, R., Eds.; Academic Press: London, 1983; Vol. 8, pp 157−220.
(11) Whitfield, M.; Turner, D. R. In *Aquatic Surface Chemistry: Chemical Processes at the Particle−Water Interface*; Stumm, W., Ed.; John Wiley & Sons: New York, 1987; pp 457−493.

10.1021/ac034227z CCC: $25.00
Published on Web 06/28/2003

measurements of trace metal contents of phytoplankton from natural waters[12−15] and none of other protists. Here we describe a synchrotron-based X-ray fluorescence (SXRF) technique for the quantification of the elements Si, Mn, Fe, Ni, and Zn in individual aquatic protists. In addition to quantifying and mapping these elements in single cells, SXRF simultaneously measures cellular constituents such as P, S, K, and Ca that may serve as markers of organelles. Two-dimensional maps of element distributions can be compared with light and epifluorescence micrographs to further elucidate the role of these elements in cellular functions.

X-ray spectrometry has been used for more than half a century to both identify and quantify the elemental composition of a wide variety of geological, biological, and manufactured targets.[16] A range of ionizing radiation has been employed to induce characteristic X-ray emission, including electrons, protons, and X-rays produced by radioisotopes, vacuum X-ray tubes, and synchrotron radiation; each has its own advantages. Electrons are particularly easy to generate and focus, so electron microprobes are widely available. However, side-scattering can significantly increase the excited area to 100 nm^2 or more, irrespective of the electron beam size.[17] In addition, electrons generate a significant bremsstrahlung background, which leads to lower trace element sensitivity, lower signal-to-noise ratio, and thus higher radiation dose for detecting a specified trace element concentration.[18] Protons are less easy to generate and focus, but their significantly higher momentum relative to electrons leads to less side-scattering and bremsstrahlung; however, it also leads to relatively high radiation dose.[18] X-rays undergo almost no side-scattering and generate little bremsstrahlung (only indirectly, through electrons resulting from X-ray absorption and inelastic scattering). As a result, X-rays offer high sensitivity and low radiation dose simultaneously.

Currently, hard (>1 keV) X-ray microprobes that employ Fresnel zone plates[19,20] to focus incident X-rays can achieve submicrometer spatial resolution even on comparatively thick (e.g., 10−20 μm) samples. However, a high-brilliance X-ray source, such as the Advanced Photon Source at Argonne National Laboratory, is required to provide adequate flux of spatially coherent photons in the appropriate photon energy range. Because of their lower absorption cross sections, X-rays penetrate deeper into the sample than electrons, permitting synoptic analyses of entire cellular targets without sectioning or otherwise altering the cells. The attenuation length of 10-keV X-rays in the organic material of target cells (equivalent to 0.187 g cm^{-3} polyimide—see Supporting Information) is 18.1 mm; therefore, only 0.06% of incident X-rays are absorbed by a 10-μm-thick target cell. Matrix effects such as the self-absorption of fluorescence photons are minimal for individual cells such as aquatic protists.[21,22] Sample calculations indicate that only 5% of Si Kα photons and <1% of Mn, Fe, Ni, and Zn Kα emissions would be absorbed by the organic material of a 10-μm cell. Further, the siliceous frustule of a 12-μm diatom would absorb <1% of the characteristic Kα photons of all elements between Si and Zn (see Supporting Information for specifics of these calculations).

The high elemental sensitivity and spatial resolution of SXRF microprobes make them well-suited for studying the interactions of trace metals and single cells in natural systems. By focusing on individual cells with unique taxonomy or morphology, microprobe analyses complement bulk measurements performed on size-fractionated filtered samples. In fact, electron and proton microprobes have been used previously to measure the macronutrient (e.g., N, P, Si) content of natural aquatic protists,[23,24] but they lack the combination of spatial resolution and sensitivity required to analyze trace metal contents in naturally occurring cells (with the exception of rare metal-sequestering bacteria[25]). SXRF has been used to map and quantify Mn, Fe, Cu, and Zn in individual freeze-dried ovarian cells cultured directly on the analytical platform.[21,22] Here we present cell preparation and mounting steps needed to apply this analytical technique to free-living marine protists collected from natural environments. While NIST thin-film standards are used to convert fluorescence counts to element concentration, independent biological standard reference materials with micrometer-scale homogeneity are not yet available for SXRF.[26] Therefore, we also compared elemental analyses of cultured aquatic protists using SXRF with GFAAS analyses to evaluate the accuracy of the SXRF results.

EXPERIMENTAL SECTION

Cleaning of Material and Reagents. Historically, measurements of trace elements in aquatic samples have been fraught with contamination artifacts, so strict protocols were followed to ensure that samples were not contaminated during preparation and mounting. All materials that came into contact with cells (or cell suspensions) were made of either polyethylene or Teflon (with the exception of the Au electron microscopy grids). Plastic-ware was soaked in Micro detergent (∼1%) overnight, rinsed thoroughly with 18-MΩ Milli-Q water, soaked in 1 M HCl (reagent grade) for 1 week, rinsed with Milli-Q water, soaked in 0.05 M HCl (trace metal grade), and rinsed with Milli-Q water prior to drying in a class-100 laminar-flow clean-air bench. All culture manipulations were performed in a class-100 laminar-flow clean-air bench as well. Glutaraldehyde (50%, electron microscopy-grade, Electron Microscopy Sciences) was diluted with Milli-Q water to a final concentration of 10% and buffered (pH 8) with 1 M NaOH (SupraPur). The solution was passed through Dowex 50-W cation-

(12) Martin, J. H.; Knauer, G. A. *Geochim. Cosmochim. Acta* **1973**, *37*, 1639−1653.
(13) Collier, R.; Edmond, J. *Prog. Oceanogr.* **1984**, *13*, 113−199.
(14) Sañudo-Wilhelmy, S. A.; Kustka, A. B.; Gobler, C. J.; Hutchins, D. A.; Yang, M.; Lwiza, K.; Burns, J.; Capone, D. G.; Raven, J. A.; Carpenter, E. J. *Nature* **2001**, *411*, 66−69.
(15) Cullen, J. T.; Sherrell, R. M. *Mar. Chem.* **1999**, *67*, 233−247.
(16) Jenkins, R.; Gould, R. W.; Gedcke, D. *Quantitative X-ray Spectrometry*, 2nd ed.; Marcel Dekker: New York, 1995.
(17) Sparks, C. J. In *Synchrotron Radiation Research*; Winick, H., Doniach, S., Eds.; Plenum Press: New York, 1980; pp 459−512.
(18) Kirz, J.; Sayre, D.; Dilger, J. In *Short Wavelength Microscopy*; Parsons, D. F., Ed.; NY Academy of Science: New York, 1978; Vol. 306, pp 291−305.
(19) Di Fabrizio, E.; Romanato, F.; Gentili, M.; Cabrini, S.; Kaulich, B.; Susini, J.; Barrett, R. *Nature* **1999**, *401*, 895−898.
(20) Yun, W.; Lai, B.; Cai, Z.; Maser, J.; Legnini, D.; Gluskin, E.; Chen, Z.; Krasnoperova, A. A.; Vladimirsky, Y.; Cerrina, F.; Di Fabrizio, E.; Gentili, M. *Rev. Sci. Instrum.* **1999**, *70*, 2238−2241.
(21) Bohic, S.; Simionovici, A.; Ortega, R.; Heymann, D.; Schroer, C.; Snigirev, A. *Nucl. Instrum. Methods Phys. Res. B* **2001**, *181*, 728−733.
(22) Bohic, S.; Simionovici, A.; Snigirev, A.; Ortega, R.; Deves, G.; Heymann, D.; Schroer, C. G. *Appl. Phys. Lett.* **2001**, *78*, 3544−3546.
(23) Sigee, D. C.; Levado, E.; Dodwell, A. J. *Aquat. Microb. Ecol.* **1999**, *19*, 177−187.
(24) Gisselson, L.-A.; Graneli, E.; Pallon, J. *Limnol. Oceanogr.* **2001**, *46*, 1237−1242.
(25) Heldal, M.; Fagerbakke, K. M.; Tuomi, P.; Bratbak, G. *Aquat. Microb. Ecol.* **1996**, *11*, 127−133.
(26) Zeisler, R. *Fresenius J. Anal. Chem.* **1998**, *360*, 376−379.

exchange resin (50X4−400; H-form), prepared as outlined by Price et al.,[27] at 1 mL min^{-1} to remove trace metal impurities and stored in the dark at 4 °C until use. We determined that there was no loss of glutaraldehyde during passage through the cation-exchange resin by monitoring absorbance of the solution at 280 nm.[28]

Sample Preparation. Target cells were mounted on Au transmission electron microscopy grids (London Finder Grids, Electron Microscopy Sciences) coated with a thin film of pure Formvar resin stabilized with evaporated C film. The C/Formvar film is approximately 50−100 nm thick, has low levels of trace metal impurities, and is optically transparent, allowing cells to be identified with light and epifluorescence microscopy prior to SXRF analysis. London Finder grids carry labels that are opaque to the incident X-rays. This allows identification of each individual grid square, so that individual target cells can be relocated in the microprobe. Finder grids can be purchased with a wide range of mesh sizes, allowing the grids to be matched to the size of the target cells.

Cultured cells were concentrated with gentle centrifugation (438*g*) onto grids in polyethylene centrifuge tubes fit with molded Araldite bases. The supernatant was gently decanted, and the grids were immediately removed with Teflon-coated forceps and allowed to dry in a darkened laminar-flow bench. For cells suspended in saline solution such as seawater, it is necessary to rinse off residual saline media to prevent formation of salt crystals that greatly increase background X-ray fluorescence and visually obscure target cells. To protect delicate cells from lysing during rinsing with Milli-Q water, cells were preserved with 0.25% buffered glutaraldehyde immediately prior to centrifugation. Following centrifugation, the grids were held in Teflon-coated forceps and gently rinsed with several drops of Milli-Q water. After drying for 15 min, the grids can be examined and photographed with both transmitted light and epifluorescence microscopy (dry objectives) soon after mounting. Once the targets have been logged, the dried grids can be stored in a desiccator until SXRF analysis.

SXRF Targeting and Analysis. Samples were analyzed at the 2-ID-E hard X-ray microprobe at the Advanced Photon Source, Argonne National Laboratory (Argonne, IL). The grid was placed on a kinematic specimen holder developed for both a light microscope and the X-ray microprobe. The holder was then mounted on a Leica DMXRE light microscope, and target cells were precisely located on the grid relative to a reference point using a high spatial resolution motorized x/y stage (Ludl Bioprecision) with an encoder resolution of 0.1 μm, a repeatability of 0.75 μm, and an accuracy of 3.0 μm over a 77 mm × 51 mm travel range. The grid was then transferred to the microprobe where the same cells were relocated using the coordinates determined from the light microscope (<2.0-μm error). The specimen chamber of the X-ray microprobe was filled with He to replace Ar in the chamber atmosphere and increase sensitivity to X-ray fluorescence from low-*Z* elements. A tunable, monochromatic X-ray beam from an undulator X-ray source was focused to a spot of approximately 0.7 μm × 0.5 μm full width at half-maximum (fwhm). The fwhm represents the beam diameter at 50% of maximum measured flux intensity, and a spot of these dimensions will contain 50% of all focused X-ray flux. The depth of focus is 300 μm, ensuring that the entire cell is in focus. An incident photon energy of 10 keV was chosen to allow excitation of Kα X-ray fluorescence in elements with atomic numbers between $Z = 13$ (Al) and $Z = 30$ (Zn). The sample was scanned through the focused beam, and the entire X-ray fluorescence spectrum was recorded at each pixel using an energy-dispersive, three-element germanium detector optimized for low-*Z* detection (Canberra Ultra-LEGe detector). The pixel step size was set to 0.5 μm, but dwell times were varied to ensure adequate counting statistics (typically 2 s). This step size provides some oversampling, ensuring that no areas of the target were missed. Elemental maps were generated from the 3D SXRF data sets (*x*, *y*, energy) by spectral filtering. For example, the map for Ca was generated by integrating over the SXRF spectrum from typically 3.59 to 3.79 keV, well matched to the Ca Kα line at 3.69 keV.

Spectral Analysis and Elemental Quantification. The spectra were summed over the area of the cell, which was identified by the Ca Kα fluorescence map since Ca is an abundant element in these aquatic organisms.[29] The integrated target spectrum was then corrected for background fluorescence from the C/Formvar support film (generally <10% of cell fluorescence). The quantification of trace constituents in target cells with complex elemental matrixes has required improvements in the acquisition and analysis of spectral data, and we have developed a protocol for modeling the fluorescence spectra of the pixels representing the cell. Spectral modeling has been used by some electron microprobe researchers,[30] but we are not aware of its prior use with submicrometer-resolution hard X-ray fluorescence microprobes. The model accounts for overlaps in the fluorescence peaks of neighboring elements, such as Mn Kβ−Fe Kα and Zn Kα−Cu Kβ (K-shell electrons excited by incident X-rays emit fluorescence photons at several energies, producing both Kα and Kβ peaks), and other properties of the acquired spectra that make a direct quantification of the measured elemental content difficult.

Using a Marquardt−Levenberg iterative search algorithm in Matlab (version 5.3, MathWorks Corp), background-corrected spectra were fit to a summed exponentially modified Gaussian (EMG) peak model with a sigmoidal baseline (tolerance 0.000 01). In its raw form, this model contains 150−200 parameters, depending on the incident energy of the excitation beam. Such complex formulations of peaked distributions are often difficult to fit to data; to reduce the problem to a tractable size, several constraints and simplifications were employed. First, a single standard deviation (peak width) was fit for all peaks. The ratios of the amplitudes of the elemental Kα and Kβ emission lines were also tightly constrained to conform to well-established values.[31] Finally, we presumed that the relative positions of the peak midpoints matched those established previously for X-ray fluorescence and that differences in absolute position could be explained as a linear transformation of the vector of expected midpoints, corresponding to a shift in the detector energy calibration. These assumptions allowed us to center all 20 peaks of interest using only two

(27) Price, N. M.; Harrison, G. I.; Hering, J. G.; Hudson, R. J.; Nirel, P. M. V.; Palenik, B.; Morel, F. M. M. *Biol. Oceanogr.* **1988**/**1989**, *6*, 443−461.
(28) Gillett, R.; Gull, K. *Histochemistry* **1972**, *30*, 162−167.
(29) Frausto da Silva, J. R. R.; Williams, R. J. P. *The Biological Chemistry of the Elements: The inorganic chemistry of life*; Oxford University Press: Oxford, U.K., 1991.
(30) LeFurgey, A.; Davilla, S. D.; Kopf, D. A.; Sommer, J. R.; Ingram, P. *J. Microsc. (Oxford)* **1992**, *165*, 191−223.
(31) Van Grieken, R. E.; Markowicz, A. A. *Handbook of X-ray Spectrometry: Methods and Techniques*; Marcel Dekker: New York, 1993.

parameters, an offset factor and a multiplier (slope). The sigmoidal baseline was employed to empirically account for background in the detector. Baseline estimation is not a problem at the higher end of the spectrum where relative background fluorescence is lower and the peaks are more widely spaced. In all, 29 parameters were allowed to float unconstrained during the fitting process. The models and data were square root transformed before fitting to stabilize variance and reduce the influence of large peaks on the solution.

Element concentrations (μg cm^{-2}) were then calculated from peak areas using peak area:concentration ratios determined from NIST thin-film standards (SRM 1832 and 1833). While NIST thin-film standards were used to convert X-ray fluorescence to element concentration, additional standard reference materials optimized for XRF analysis in microprobes are not available for independent confirmation of the accuracy of the microprobe. Therefore, we prepared our own set of standards for the elements Si and Fe. Separate dilution series of $FeCl_3$ and Na_2SiO_3 solutions were prepared, and 1 μL of each solution was dried onto separate acid-washed 25-mm-diameter 0.2-μm polycarbonate membranes (Nuclepore). The entire area of each dried standard solution was scanned in the microprobe, fluorescence counts summed in the Si and Fe spectral channels, and background fluorescence counts from the membranes subtracted (the Fe signal from the blank filter accounted for 31% of the signal in the lowest Fe standard).

Analytical Precision. Many variables influence the precision, and, hence, the detection limits, of the SXRF technique; these factors include the beam conditions (focused photon flux and incident energy), detector placement, overall background fluorescence from the sample chamber, and target analysis parameters (step size, dwell time). Sample preparation can also affect the background element concentrations on the C/Formvar support film. Finally, the precision with which the measured characteristic fluorescence is quantified will be governed by a combination of counting statistic considerations and the quality of the spectral model fit.

To assess the precision of the entire quantification technique, we performed three independent scans of the same autotrophic dinoflagellate, as well as duplicate measurements on each of four other cells (two centric diatoms and two heterotrophic dinoflagellates). The cells were collected from the Southern Ocean (20 m) during the Southern Ocean Fe Experiment (SOFeX) using trace metal clean techniques. Whole water samples were obtained from Teflon-lined GO-FLO bottles mounted on a plastic-coated rosette[32] used to collect water for bulk trace metal analyses. Water was gently transferred directly into acid-washed polycarbonate bottles and transferred to a class-100 laminar-flow hood, where the natural plankton assemblage was mounted on Au grids as described above. Before each scan, the cells were retargeted in the microprobe, and the collected fluorescence spectra were independently averaged and modeled.

Detection Limits. Focusing simply on the issue of background (= blank) element variability, the minimum detection limits (MDL) can be calculated as 3 × SD of the element concentrations in the background support film. This was done for the background regions (n = 15) on a grid mounted with Southern Ocean cells. Background regions on the *Thalassiosira weissflogii* and *Stephanodiscus hantzschii* grids were not used for this calculation since both have elevated element concentrations resulting from the culture media.

We have also estimated the minimum detection limit based on counting statistics. Like all discrete random events, SXRF fluorescence counts are Poisson distributed—i.e., the estimated total number of counts, n, and the associated variance are equivalent.[16] Thus, following the rule of variance propagation for addition operations, the variance of a background-corrected count from a cell, n_c, is the sum of the target, n_t, and background, n_b, counts. If, for simplicity, we assume the target and background regions have the same number of pixels, the coefficient of variation (CV) of n_c is estimated by

$$\mathrm{CV} = \frac{(n_t + n_b)^{0.5}}{(n_t - n_b)} = \frac{(n_c + 2n_b)^{0.5}}{n_c} \qquad (1)$$

We can alter eq 1 to solve for the minimum detection limit (for $\mu = n_c = 3\sigma$ or CV = $^1/_3$). We first relate n_c to the cellular metal content, $[X]_c$ (g cell^{-1}), the fluorescence yield for that element, ω_X ((counts s^{-1})/(g cm^{-2})), the apparent area of the cell, A_c (cm^2), the number of pixels within the region of the cell, p, and the dwell time for each pixel, t_d (s pixel^{-1}). Substituting, rearranging, and setting CV to $^1/_3$, we can then solve for the value of X_c that corresponds to the MDL (see Supporting Information for details):

$$X_c = \frac{9}{2}\left(1 + \left(1 + \frac{8}{9}n_b\right)^{0.5}\right)\left(\frac{A_c}{\omega t_d p}\right) \qquad (2)$$

The background count rate, n_b, varies, so we use the 95th percentile of the background count rates observed for the Southern Ocean samples to ensure a 95% chance of achieving the given CV no matter where the target cell is located on the grid.

XRF-GFAAS Intercomparison. While NIST standards, augmented by our own standards, were used to quantify the elements in each cell with SXRF, appropriate SRMs are not available for testing of the whole technique (including cell fixation, mounting, and drying prior to SXRF). Therefore, freshwater and marine diatoms were cultured and analyzed with both SXRF and GFAAS to provide an independent measure of the SXRF values. The freshwater diatom *S. hantzschii* (clone UTCC 267) was grown in WCL-1 media[33] and the coastal marine diatom *T. weissflogii* (CCMP 1336) was grown in 0.22-μm filtered coastal North Atlantic seawater enriched with f/2 levels of nitrate, phosphate, silicate, and vitamins.[33] Both species were cultured in acid-washed glass Erlenmeyer flasks at 150 μmol quanta m^{-2} s^{-1} on a 14:10 h light/dark cycle, *S. hantzschii* at 20 °C and *T. weissflogii* at 16 °C. Cells were harvested at the end of log-phase growth by centrifugation onto grids as described above. Additionally, an aliquot of *S. hantzschii* was mounted without glutaraldehyde fixation for comparison to the fixed treatment. Aliquots of each culture were also collected on acid-cleaned membrane filters (1 μm for *S. hantzschii*, 3 μm for *T. weissflogii*) for subsequent bulk analysis of Si, Mn, Fe, Ni, and Zn. Aliquots of both cultures were filtered

(32) Johnson, K. S.; Elrod, V. A.; Fitzwater, S. E.; Plant, J. N.; Chavez, F. P.; Tanner, S. J.; Gordon, R. M.; Westphal, D. L.; Perry, K. D.; Wu, J.; Karl, D. M. *Global Biogeochem. Cycles*, in press.

(33) Guillard, R. R. L. In *Culture of Marine Invertebrate Animals*; Smith, W. L., Chanley, M. H., Eds.; Plenum: New York, 1975; pp 29−60.

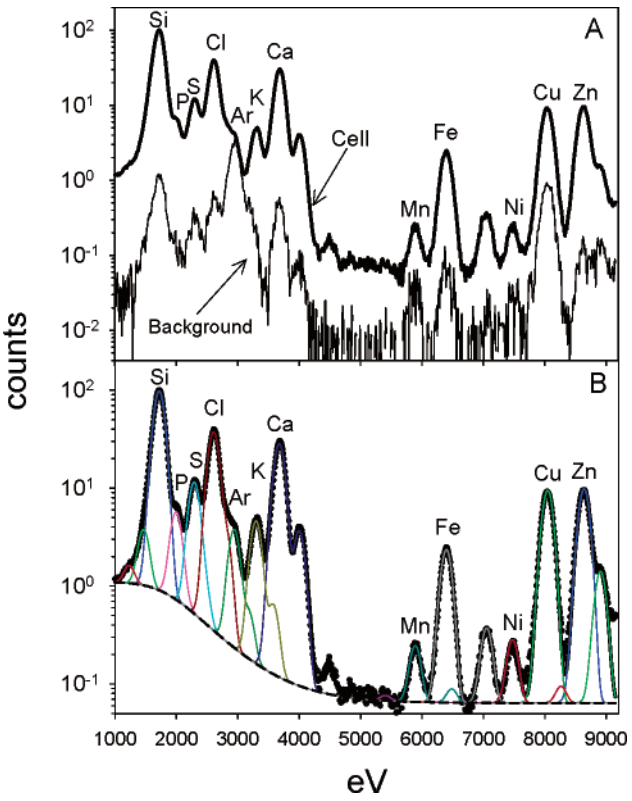

Figure 1. Fluorescence spectra for the marine diatom *T. weissflogii*. Pixel-averaged spectra for the target cell and a neighboring background region are plotted in (A). The Kα peaks of the major bioactive elements are indicated above the peaks. (B) displays the fit of the EMG model to the cell spectrum. The sigmoidal baseline is shown as a dotted line, the overall model is black, and the Kα and Kβ peaks for each element are displayed in various other colors.

through combusted GF/F filters for bulk C analysis. For all bulk analyses, uninoculated media were passed through clean filters to correct for element adsorption directly to the filters.

Bulk C, Si, and Trace Metal Analyses. Carbon analysis of the GF/F filters was performed with a Carlo-Erba EA-1102 elemental analyzer, standardized with sulfanilamide. Biogenic Si was measured spectrophotometrically[34] following digestion with NaOH.[35] Total cellular Mn, Fe, Ni, and Zn contents were obtained using standard addition protocols in a GFAAS (PE AAnalyst 800) after a sequential acid treatment (0.75% HCl, 0.25% HNO_3, 0.05% HF) in Teflon digestion bombs.[36] All bulk analyses were performed without knowledge of the corresponding SXRF results, eliminating analyst bias.

RESULTS AND DISCUSSION

Spectral Analysis. Figure 1A shows X-ray fluorescence spectra for a typical *T. weissflogii* cell and the cell's neighboring background region. The Si, P, S, Cl, K, Ca, Mn, Fe, Ni, and Zn Kα peaks are significantly elevated within the cell (note the log scale). While some of these peaks are also present in the background, only Ar and Cu appear at comparable levels. The Ar peak, which results from residual air in the He-filled sample chamber, is identical in the two spectra. The high Cu fluorescence in the background is likely due to contamination introduced by the grid bars, as direct SXRF analysis of the Au EM grids reveals notable Cu (but not Si, Mn, Fe, or Zn) content. We believe that Cu from the Au grids is contaminating the C/Formvar film and the cells themselves during the aqueous phase of cell mounting. Cells analyzed with SRXF show Cu concentrations 10−100-fold higher than cells analyzed with GFAAS. Because of this artifact, we believe the Cu SXRF results are not reliable, and we are currently searching for grids that are free of Cu contamination but still opaque to the incident X-rays (necessary for locating target cells).

The modeled X-ray peaks are superimposed on the cell spectrum in Figure 1B. The sigmoidal baseline is evident at the lower end of the spectrum. This fitted baseline accounts for an approximate 10-fold increase in detector background in this region of the spectrum, but this correction accounts for <1% of the area of the Si Kα peak. More importantly, the EMG model corrects for overlapping Kα and Kβ peaks of neighboring elements. The close proximity of the Si, S, P, and Cl Kα peaks results in overlap that is accounted for by the model. At the higher energies, the model corrects for the overlap of Mn Kβ and Fe Kα, Ni Kβ and Cu Kα, and Cu Kβ and Zn Kα.

Detection Limits. The calculated MDL for this SXRF microprobe are shown in Table 1. Unlike GFAAS and ICPMS MDLs, which are usually reported as volume concentrations, the microprobe MDLs are reported as areal concentrations. For each element, we have taken two approaches to calculating the MDL. Calculated as 3 × SD of 15 background scans, the MDL is 7.0×10^{-16} mol μm^{-2} for Si and between 5.0×10^{-20} and 3.9×10^{-19} mol μm^{-2} for Mn, Fe, Ni, and Zn. For these trace metals, which have low backgrounds and high fluorescence yields, SXRF is therefore capable of detecting subattomole per square micrometer concentrations. The MDLs calculated from counting statistics are similar to—although generally lower than—those calculated from the variability in the backgrounds (= blanks). A comparison of hypothetical small (3 μm) and large (20 μm) cells demonstrates that larger cells have lower MDLs since there is more biomass per area (the cells are three-dimensional targets projected onto a two-dimensional field), hence higher counts and greater precision.

The MDLs have also been converted to minimum detectable cellular concentrations (mol $cell^{-1}$; Table 1) to facilitate comparison of SXRF sensitivity with published quotas for aquatic protist cells. Calculated this way, MDLs for small cells are lower than those for large cells, a result that seems counterintuitive since the smaller cells have much less cellular material overall. However, at a given cellular elemental content, there is more metal per area for a small cell than for a large cell because average cell thickness is proportional to cell radius, whereas cell area is proportional to the square of the cell radius. Moreover, in our comparison, the total amount of time spent analyzing the target is kept approximately equivalent for all cells by adjusting detector dwell time to account for the varying number of pixels covering the target. The MDL for Fe in a single 3-μm plankton cell is calculated to be 2 amol $cell^{-1}$. Given that Sunda and Huntsman[6] measured the Fe quotas of the oceanic protists *Emiliania huxleyi* (3 μm) and *Thalassiosira oceanica* (5−6 μm) to be approximately 1.3 and 2.7 amol $cell^{-1}$, respectively, it is apparent that the SXRF microprobe

(34) Parsons, T. R.; Miata, Y.; Lalli, C. M. *A Manual of the Chemical and Biological Methods for Saltwater Analysis*; Pergamon Press: New York, 1984.
(35) Paasche, E. *Mar. Biol.* **1973**, *19*, 117−126.
(36) Eggimann, D. W.; Betzer, P. R. *Anal. Chem.* **1976**, *48*, 886−890.

Table 1. Minimum Detection Limits of Si, Mn, Fe, Ni, and Zn[a]

	background (3 × SD)	small cell diam = 3 μm; t_d = 4 s		large cell diam = 20 μm; t_d = 1 s	
	mol μm^{-2}	mol μm^{-2}	mol $cell^{-1}$	mol μm^{-2}	mol $cell^{-1}$
Si	7.0×10^{-16}	1.68×10^{-16}	1.18×10^{-15}	5.03×10^{-17}	1.58×10^{-14}
Mn	5.0×10^{-20}	1.54×10^{-19}	1.09×10^{-18}	4.55×10^{-20}	1.43×10^{-17}
Fe	3.9×10^{-19}	2.88×10^{-19}	2.03×10^{-18}	8.58×10^{-20}	2.70×10^{-17}
Ni	5.3×10^{-20}	1.03×10^{-19}	7.27×10^{-19}	3.05×10^{-20}	9.57×10^{-18}
Zn	2.8×10^{-19}	1.50×10^{-19}	1.06×10^{-18}	4.49×10^{-20}	1.41×10^{-17}

[a] Calculated as 3 × SD of the background regions or calculated from a consideration of counting statistics for two different hypothetical cells.

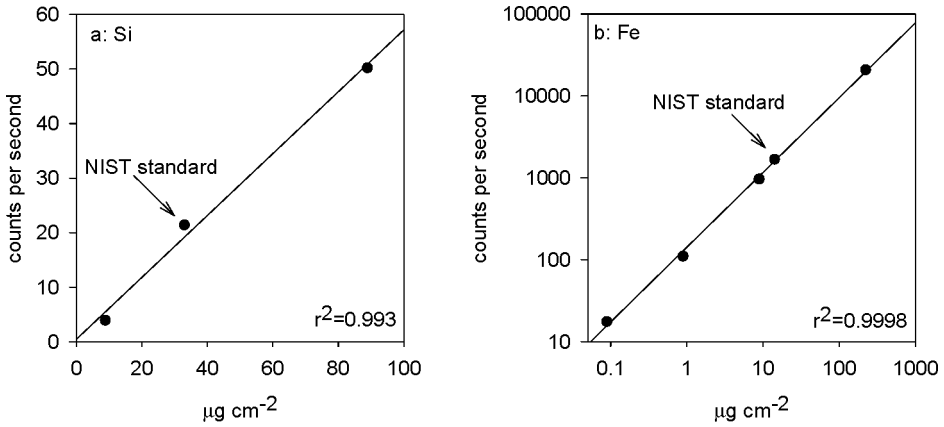

Figure 2. Standard calibration curves for Si and Fe. Both figures plot fluorescence counts against the areal concentration of the element on a thin-film standard. The standards were prepared from liquid solutions of known concentration, with the exception of one NIST standard. Note the log scale of the axes in panel b.

can detect Fe at physiologically critical cellular concentrations even in cells as small as 3 μm. The MDL of the SXRF microprobe can be further extended to encompass even smaller cells by increasing detector dwell time; this would increase sample analysis time and the possibility of radiation damage to the sample, although metal concentrations should remain unaffected.

Standards. The calibration curves generated for Si and Fe are presented in Figure 2. Both standard series show a linear detector response over the measured ranges (4-fold range for Si, 1000-fold range for Fe), with $r^2 > 0.99$ for both elements (note that the Si calibration curve is composed of only three data points). The Si concentrations (on an areal basis) of both *S. hantzschii* and *T. weissflogii* fall within the range of the standards, as does the Fe concentration of *S. hantzschii* (*T. weissflogii* Fe concentrations are slightly lower: 0.02 μg cm^{-2}). In addition to confirming linear detector response, these standards provide an independent verification of the areal Si and Fe concentrations in the NIST standards used to convert X-ray fluorescence counts to element density.

Precision. The precision of the entire SXRF quantification technique was assessed with repeated analyses of a single target. Five different marine protists collected from the Southern Ocean (two centric diatoms, one autotrophic dinoflagellate, two heterotrophic dinoflagellates) were each analyzed multiple times, and the results are presented in Table 2. The CVs for repeated analyses were <5% for Si, Mn, Fe, and Zn and <10% for Ni, despite the fact that only femtomole-to-picomole amounts of elements were analyzed in each cell. By comparison, the CVs of replicate filters analyzed by GFAAS were higher, ranging from 8.6% for Mn to 162% for Zn. These results demonstrate that the overall SXRF analysis procedure, from cell targeting to fluorescence detection to model fitting to background correction, has the precision needed for environmental analyses. As with the MDLs, the precision can be increased by increasing detector dwell times.

SXRF-GFAAS Intercomparison. Use of the WCL-1 media resulted in higher Mn and Fe MDLs and lower Si, Ni, and Zn MDLs than calculated for the Southern Ocean samples. The MDLs calculated for the *S. hantzschii* grids were 5.6×10^{-17} mol μm^{-2} Si, 1.4×10^{-19} mol μm^{-2} Mn, 1.2×10^{-17} mol μm^{-2} Fe, 1.1×10^{-20} mol μm^{-2} Ni, and 2.1×10^{-20} mol μm^{-2} Zn. The cellular contents (mol $cell^{-1}$) of Si, Mn, Fe, and Zn in *S. hantzschii* as measured by spectrophotometry, GFAAS, and SXRF are shown as box plots in Figure 3. Cellular Ni, which was below the detection limit of both GFAAS and SXRF, is not shown. For all four elements, the cellular content as determined with GFAAS on filtered samples (aggregating millions of cells) was similar to that using single-cell SXRF. The only significantly different (*t*-test, $P < 0.05$) treatment was found with Fe. SXRF measurements of Fe in DI-rinsed cells were slightly lower than both glutaraldehyde-fixed cells analyzed with SXRF and DI-rinsed cells analyzed with GFAAS (DI-rinsed GFAAS cells were not different from fixed SXRF cells).

A comparison of the element contents of the glutaraldehyde-preserved cells with those left unfixed reveals no notable differences (Figure 3). Glutaraldehyde penetrates cellular membranes and cross-links proteins, and two possible artifacts may be introduced during chemical fixation: internal elements may leach out of the cell when membranes are compromised, and contaminant elements may be introduced to the cell with the glutaraldehyde. The glutaraldehyde was stripped of metal contaminants with

Table 2. Mean Total Elements and Coefficients of Variation ((SD ÷ mean) × 100) in Target Cells and Filters for Replicate Measurements of Aquatic Protists As Measured with SXRF and GFAAS[a]

	SXRF: single-cell analysis (g cell^{-1})						GFAAS: filter analysis (g filter^{-1})	
	diatom ($n = 2$)	diatom ($n = 2$)	A. dino.[b] ($n = 3$)	H. dino.[b] ($n = 2$)	H. dino. ($n = 2$)	mean CV	*Stephanodiscus* ($n = 8$)	*Thalassiosira* ($n = 4$)
Si	2.78×10^{-11}	9.39×10^{-11}	nd[b]	nd	1.02×10^{-12}		4.86×10^{-5}	5.65×10^{-5}
% CV	0.2	2.4			3.9	2.2	0.3[c]	1.6[d]
Mn	3.20×10^{-16}	nd	nd	7.72×10^{-15}	4.20×10^{-16}		3.60×10^{-8}	5.79×10^{-9}
% CV	6.0			5.0	3.5	4.8	8.6	35.2
Fe	1.91×10^{-14}	1.10×10^{-14}	5.13×10^{-15}	1.31×10^{-13}	1.91×10^{-15}		2.01×10^{-6}	2.92×10^{-7}
% CV	0.9	1.5	4.0	6.0	8.0	4.1	14.9	12.8
Ni	3.09×10^{-15}	nd	5.67×10^{-15}	2.56×10^{-14}	nd		nd	2.71×10^{-9}
% CV	5.9		4.9	7.3		6.0		33.5
Zn	1.33×10^{-15}	6.62×10^{-15}	6.82×10^{-15}	1.51×10^{-13}	1.19×10^{-14}		1.22×10^{-8}	4.47×10^{-8}
% CV	0.9	8.3	1.5	5.2	6.2	4.4	161.7	81.4

[a] For SXRF analyses, n is the number of replicate measurements of each cell; a total of two diatom cells, two heterotrophic dinoflagellate cells, and one autotrophic dinoflagellate cell was analyzed. For GFAAS analyses, n is the number of replicate filters analyzed. [b] A. dino., autotrophic dinoflagellate; H. dino., heterotrophic dinoflagellate; nd, not detectable. [c]Measured with UV spectrophotometry ($n = 2$). [d]Measured with UV spectrophotometry ($n = 3$).

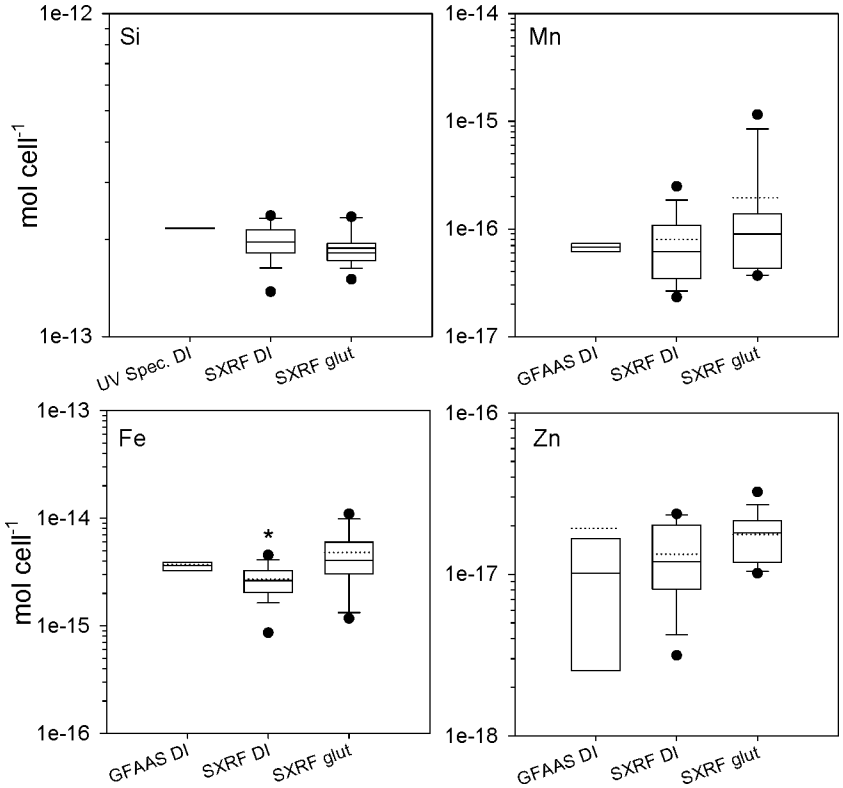

Figure 3. Si, Mn, Fe, and Zn contents of *S. hantzschii* cells as measured by UV spectrophotometry, GFAAS, and SXRF. The cells analyzed with spectrophotometry ("UV Spec. DI", $n = 2$ filters) and GFAAS ("GFAAS DI", $n = 8$ filters) were collected on filters and rinsed with deionized water. Cells analyzed with SXRF were treated the same way ("SXRF DI", $n = 16$ cells), but an additional treatment was fixed with glutaraldehyde prior to centrifugation ("SXRF glut", $n = 15$ cells). In these plots, the solid line represents the median, the dotted line is the arithmetic mean, the box delineates the 25th and 75th percentile confidence intervals, and the error bars encompass the 10th and 90th percentile confidence intervals. Data falling outside of these ranges are plotted individually. Treatments found to be significantly different (t-test, $P < 0.05$) are noted with an asterisk (*).

cation-exchange resin prior to use, reducing the likelihood of the latter artifact. The good agreement between the element contents of fixed and unfixed cells suggests that fixation did not allow elements to leach from the cells prior to drying. In fact, by stabilizing cell structure, the chemical fixative may enhance retention of elements that might otherwise have leached during the rinsing and drying process. It appears that this is what has happened with Fe, where the SXRF results for fixed cells most closely match the GFAAS results. The unfixed cells analyzed with SXRF have lost Fe present in both the GFAAS-analyzed cells and the fixed SXRF cells. While we cannot unequivocally disprove that cellular elements are leached during sample preparation, the

similarity in element concentrations between the unfixed GFAAS cells and the fixed SXRF cells suggests that this process does not appreciably affect the whole-cell results.

Variation in cellular metal concentrations was apparent when SXRF was used. However, the large range of values measured by SXRF represents real intercell variability in the contents of these elements—information not obtainable with GFAAS since it averages over many thousands of particles. While Si cell^{-1} is rather tightly constrained (<2-fold variation among all cells), cellular levels of the three trace metals can vary by up to 1 order of magnitude in some cases. Research with cultures has shown that trace metal contents of diatoms are far more elastic than cellular Si, which, unlike the metals, is used for structural purposes.[4,6,37] Studies employing charged particle microprobes to measure macronutrients (e.g., N, P, Si) in individual aquatic protists have also reported notable intraspecific element variability.[38,39] Gisselson et al.[24] found that the N content of individual cells of the dinoflagellate *Dinophysis norvegica* varied by a factor of 6.4, comparable to the variability in metal contents measured for *S. hantzschii*.

The cellular contents of Si, Mn, Fe, Ni, and Zn in *T. weissflogii* as measured by spectrophotometry, GFAAS, and SXRF are shown in Figure 4. The MDLs for all elements for the *T. weissflogii* cultures were ~1 order of magnitude lower than for Southern Ocean samples. As this is a marine diatom, there was no unfixed treatment—all SXRF cells were treated with glutaraldehyde prior to rinsing. SXRF and the bulk techniques produced statistically indistinguishable results (*t*-test, $P > 0.05$) for cellular Si, Mn, Fe, and Ni (which was not detectable in *S. hantzschii*). Cellular Zn was found to be significantly higher with SXRF than GFAAS (*t*-test, $P < 0.001$). The GFAAS results are within the range of cellular Zn reported in the literature for *T. weissflogii*,[4,40] but the SXRF data appear to be ~2-fold above this range. Initially it would seem unlikely that this difference was caused by glutaraldehyde contamination given that Zn contamination was not detected in fixed *S. hantzschii*, which had 10-fold lower levels of Zn on both an absolute and volume concentration basis. Additionally, prior SXRF measurements of Zn in freshwater pennate diatoms fixed with 0.25 or 2.5% uncleaned glutaraldehyde showed no significant differences (data not shown), suggesting that the glutaraldehyde did not introduce Zn contamination. The Zn added with the cleaned glutaraldehyde was calculated to be 0.5 nM, 150 times less than the concentration of Zn in the WCL-1 media, but probably within 1 order of magnitude of the Zn concentration in the enriched seawater media, which did not receive any metal additions. Given the lower ambient Zn in the seawater media, the Zn added with the glutaraldehyde may have caused the increase in cellular Zn detected by SXRF. Thus, it will be necessary to adjust the glutaraldehyde cleaning protocol to more completely remove Zn contamination before using the fixative to preserve cells from natural waters characterized by low Zn concentrations.

While the GFAAS and SXRF measurements of cellular Fe were not significantly different ($P = 0.35$), they do appear to diverge somewhat, with the SXRF-analyzed cells showing a lower median Fe concentration. Among the elements studied, Fe was unique in its highly localized distribution. In addition to the Fe that mapped onto the other cellular elements, 6 of the 16 SXRF-analyzed cells displayed very localized regions of extremely high Fe that appeared to be attached to the outside of the cells. Several examples of this are shown in Figure 5, which presents the distributions of Si, P, Fe, and Zn in five cells. In the top cell, the Fe distribution is similar to that of P and Zn, confirming that the Fe is associated with the functional units of the cell. The Fe in the second cell overlaps with P and Zn but is much more concentrated in a small spot (10−15 pixels) at the edge of the cell. The Fe here may be bound to the outside of the cell or concentrated in an intracellular Fe storage body such as ferritin. In the bottom three cells, however, the Fe maps are dominated by small spots of Fe at the edge of the cells that do not correspond

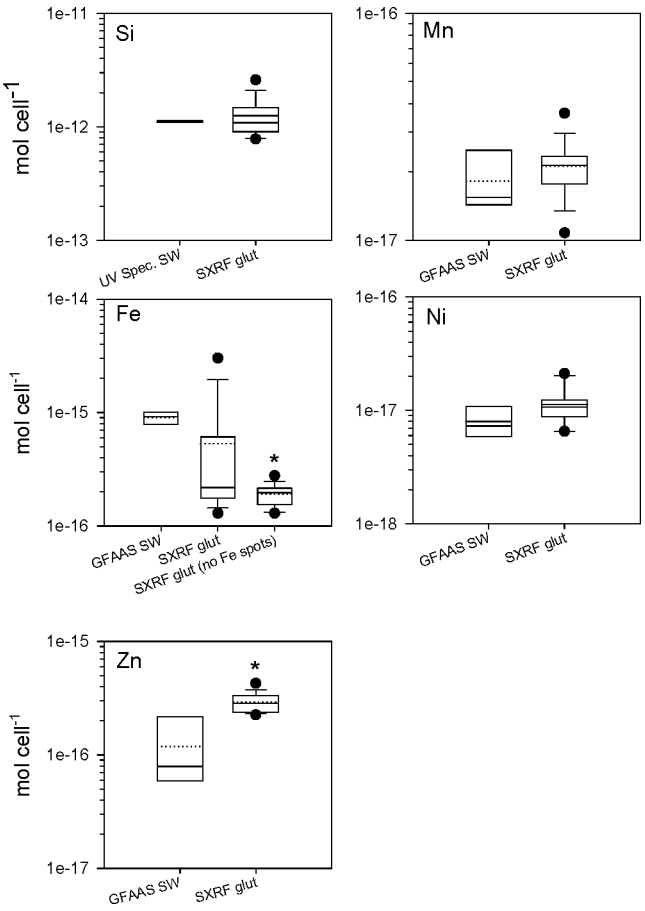

Figure 4. Si, Mn, Fe, Ni, and Zn contents of *T. weissflogii* cells as measured by UV spectrophotometry, GFAAS, and SXRF. The cells analyzed with spectrophotometry ("UV spec. SW", $n = 3$) and GFAAS ("GFAAS SW", $n = 4$) were collected on filters and rinsed with Chelexed, filtered seawater. Cells analyzed with SXRF ("SXRF glut", $n = 15$) were fixed with 0.25% glutaraldehyde prior to centrifugation. The Fe content of the same 15 cells analyzed with SXRF was also calculated without inclusion of the Fe "hot spots" and is plotted ("SXRF glut (no Fe spots)", $n = 15$). In these plots, the solid line represents the median, the dotted line is the arithmetic mean, the box delineates the 25th and 75th percentile confidence intervals, and the error bars encompass the 10th and 90th percentile confidence intervals. Data falling outside of these ranges are plotted individually. Treatments found to be significantly different (*t*-test, $P < 0.05$) are noted with an asterisk (*).

(37) De La Rocha, C. L.; Hutchins, D. A.; Brzezinski, M. A.; Zhang, Y. H. *Mar. Ecol. Prog. Ser.* **2000**, *195*, 71−79.

(38) Sigee, D. C.; Krivtsov, V.; Bellinger, E. G. *Eur. J. Phycol.* **1998**, *33*, 155−164.

(39) Krivtsov, V.; Bellinger, E. G.; Sigee, D. C. *J. Plankton Res.* **2000**, *22*, 169−184.

(40) Ahner, B. A.; Morel, F. M. M. *Limnol. Oceanogr.* **1995**, *40*, 658−665.

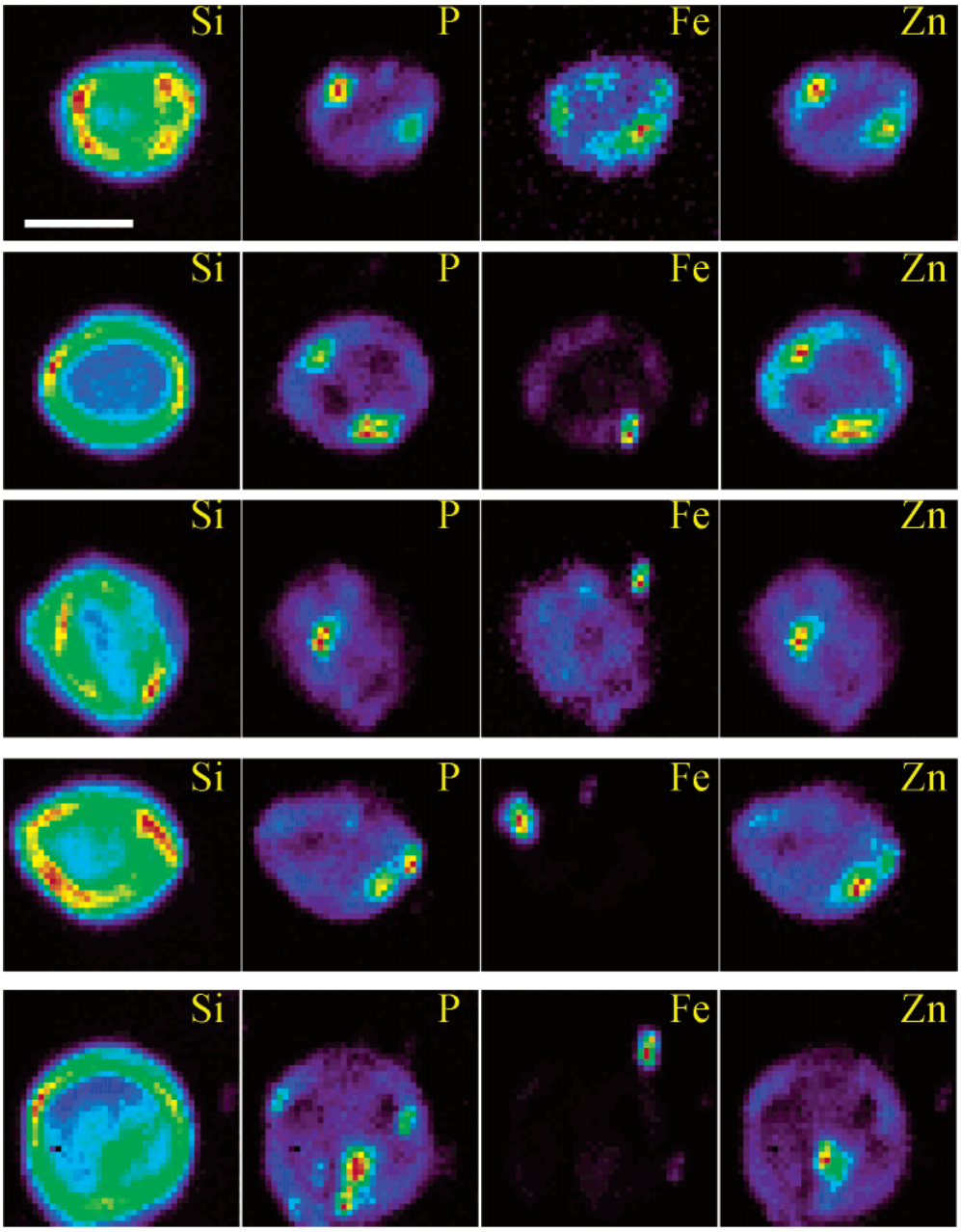

Figure 5. SXRF false-color element maps of five cultured *T. weissflogii* cells. Each image indicates the relative distribution of the specific element, and thus, the concentration scales vary for each image (scale bar 10 μm). The colors depicting elemental concentrations in each map are scaled to the maximum value for that map. Note that extremely high and localized elemental concentrations, such as in Fe "hot spots", can obscure lower elemental concentrations elsewhere in the map. The elements Si, P, Fe, and Zn in the top cell show a distribution typical of most of the cells analyzed, while the bottom four cells demonstrate the Fe "hot spots" observed in 38% of the cells analyzed.

to other cell structures. Since these Fe "hot spots" are not colocalized with areas of high P, it is unlikely that they represent ferritin, a substance characterized by high phosphorus.[41] Rather, the Fe hot spots appear to result from Fe colloids or macroparticles bound to the outside of the cells. In one case, the hot spot contained 6 times as much Fe as the rest of the cell combined. The mean Fe content of cells without hot spots was 1.9×10^{-16} mol cell^{-1}, while the mean Fe content of the cells with hot spots was 7-fold higher: 1.28×10^{-15} mol cell^{-1}. While 37.5% of the cells analyzed with SXRF had Fe hot spots, the higher median GFAAS Fe concentration suggests that this hot spot Fe was more common among the overall cell population. Given the high intercell variability in *T. weissflogii* Fe content, the 16 cells we randomly chose to analyze with SXRF would have to be representative of the overall population to produce a mean concentration comparable to that measured with GFAAS. Iron-containing particulate or colloidal matter associated with cell cultures that may be caught on the filters could also result in higher "cellular" Fe results in GFAAS analyses.

The two-dimensional nature of SXRF analyses allows us to identify and remove the pixels covering these Fe hot spots. When this was done, mean Fe cell^{-1} as measured by SXRF dropped 3-fold

(41) Nagasaka, S.; Nishizawa, N. K.; Watanabe, T.; Mori, S.; Yoshimura, E. *BioMetals* **2003**, *16*, 465−470.

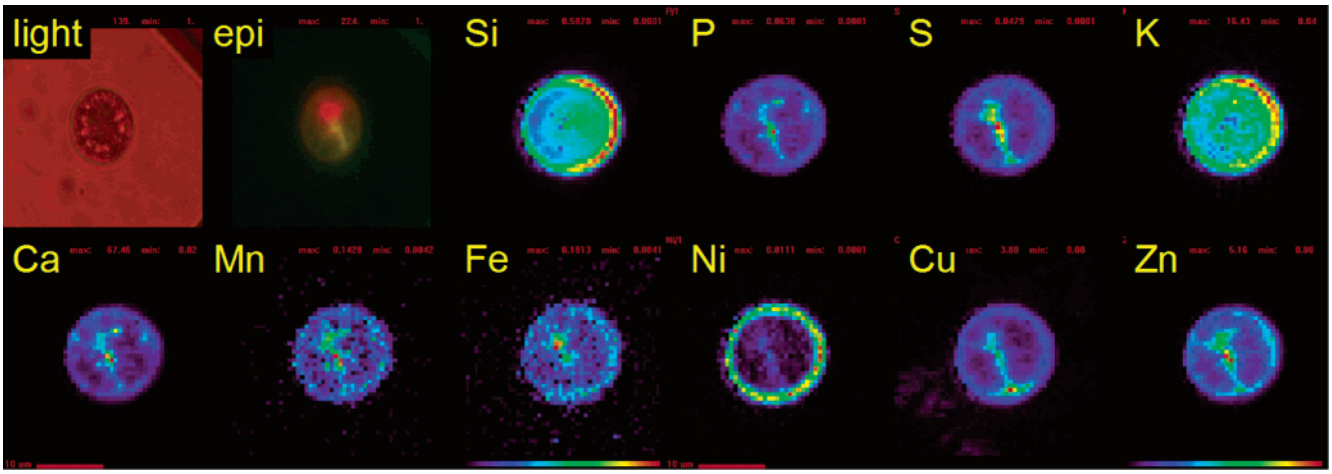

Figure 6. Light and epifluorescence micrographs and SXRF false-color element maps of a centric diatom collected from the Southern Ocean. Each SXRF image indicates the relative distribution of the specific element, and thus, the concentration scales vary for each image (red scale bars 10 μm). Si and K map onto the frustule of the cell, while P, S, Ca, Mn, Fe, Cu, and Zn appear to be associated with the cytoplasm of the cell (indicated by the green epifluorescence). Fe is most highly concentrated in the chloroplast (region of red epifluorescence), while Zn is colocalized with P (likely to be the cell's nucleus). Ni is found on the outer membranes or frustule of the cell.

(although the median Fe cell^{-1} stayed the same), and the data range shrank 10-fold (Figure 4). The mean corrected cellular Fe, normalized to cellular C (measured to be 8.6 pmol cell^{-1}), was 22.2 μmol of Fe mol C^{-1}. Sunda and Huntsman[6] reported an Fe/C ratio of 23.6 μmol of Fe (mol of C^{-1}) for *T. weissflogii* grown under low (but not growth-limiting) Fe conditions. Although our culture contained 5-fold less total Fe (22 nM) and 600-fold less EDTA (150 nM), the cells were not preacclimated to low-Fe conditions prior to the experiment and did not appear to be Fe limited (culture growth rate: 0.8 d^{-1}). Thus, it appears that the cellular Fe measured with SXRF, while slightly lower than measured with GFAAS, is reasonable for *T. weissflogii* grown at low ambient Fe.

Two-Dimensional Mapping. Beyond providing whole-cell trace element concentrations, the SXRF microprobe has the resolution to simultaneously determine the spatial distributions of elements within cells. An example of the two-dimensional element maps produced by SXRF is shown in Figure 6, accompanied by light and epifluorescence (blue excitation) micrographs of the cell. These images can be directly compared to correlate the distribution of elements with cellular structure. The target cell is a centric diatom collected from the Southern Ocean, and the siliceous outer shell of the organism is clearly delineated in the Si Kα fluorescence map. The apparent lateral gradient in Si concentration is an artifact of the angle of the cell on the support grid. While K appears to be distributed evenly throughout the cell, P, S, Ca, Mn, Fe, Cu, and Zn are localized in the internal organelles, indicated by the red and green epifluorescence. Iron is most concentrated in the chloroplast, identified by the chlorophyll *a* autofluorescence, whereas Zn is colocated with P—probably in the nucleus. The mapping ability of SXRF holds great promise for studying the mechanisms of metal bioaccumulation in aquatic protists.

In addition to providing information on the colocalization of elements within cells, the maps can be used to identify and avoid externally bound contaminants. The Fe hot spots identified in the *T. weissflogii* target cells (Figure 5) were included in the whole-cell spectra, since this Fe was also included in the GFAAS measurements. When cells collected from the field are analyzed, however, the hot spot pixels would not be included in the whole-cell spectra so as to produce more accurate measures of cellular Fe. The ability to distinguish cells from abiotic particles and account for abiotic contaminants during metal analysis is a major advantage of the X-ray microprobe in providing true cellular metal concentrations.

CONCLUSIONS

The synchrotron X-ray fluorescence microprobe can be used to precisely and accurately quantify the trace elements Mn, Fe, Ni, and Zn (as well as the macronutrient Si) in individual aquatic protist cells. By combining subattomole sensitivity with the ability to provide the two-dimensional element distributions within cells, SXRF can provide biologically relevant information not available from standard bulk techniques such as GFAAS and ICPMS. The analytical precision is better than 10%, and comparative analyses of cultured cells show the accuracy to be good. The extreme sensitivity of this approach enables clear quantitative trace element analyses of cells from all natural waters, including those most remote from human influence. Future advances should allow the measurement of Cu following replacement of the Au grids, and the introduction of trace metal "clean" cryopreservation techniques could eliminate the need for chemical fixation with glutaraldehyde. In addition, SXRF could be adapted to provide synoptic quantitative analyses of cellular element contents in other contexts beside the aquatic environment, such as soils and tissue cultures.

ACKNOWLEDGMENT

We thank Angelika Osanna, Barry Winn, Sue Wirick, and Corrie Vaa for their participation in preliminary experiments and P. Lee Ferguson and anonymous reviewers for helpful comments. The kinematic specimen holders were developed by Dan Legnini, and the CHN analyses were preformed by the Analytical Facility of the Marine Sciences Research Center. Use of the Advanced Photon Source was supported by the U.S. Department of Energy, Office of Science, Office of Basic Energy Sciences, under Contract W-31-109-Eng-38; we also thank the Department of Energy for support of preliminary experiments under Contract DE-FG02-

89ER60858. This research was supported by grants from the National Science Foundation (OPP9986069, CHE0221934, OCE9912333), the Hudson River Foundation (01199A), and the Ministry of Education of Spain. This is MSRC Contribution No. 1261.

SUPPORTING INFORMATION AVAILABLE

(1) Description of calculations made to estimate the absorption of characteristic X-rays by the target cells (matrix effects); (2) derivation of MDL equations based on Poisson counting statistics. This material is available free of charge via the Internet at http://pubs.acs.org.

Received for review March 6, 2003. Accepted May 12, 2003.

AC034227Z